# Powder X-ray diffraction data for dimethylarsinic acid, $(CH_3)_2AsO(OH)$

Joel W. Reid [a)]
*Canadian Light Source, 44 Innovation Boulevard, Saskatoon, SK, Canada S7N 2V3*

(Received 17 December 2020; accepted 7 April 2021)

Synchrotron powder diffraction data is presented for the monoclinic polymorph of dimethylarsinic acid, $(CH_3)_2AsO(OH)$ ($DMA^V$). Rietveld refinement with GSASII yielded lattice parameters of $a = 15.9264(15)$ Å, $b = 6.53999(8)$ Å, $c = 11.3401(9)$ Å, and $\beta = 125.8546(17)°$ ($Z = 8$, space group $C2/c$). The Rietveld-refined structure was compared with both a density functional theory (DFT)-optimized structure and the published, low-temperature single-crystal structure, and all three structures exhibited excellent agreement. The triclinic polymorph of $DMA^V$ was also DFT optimized with CRYSTAL17 to determine the positions of the hydrogen atoms. Monoclinic $DMA^V$ forms zigzag chains parallel to the *b*-axis with adjacent $DMA^V$ molecules connected by an O–H···O bond, whereas triclinic $DMA^V$ forms dimers connected by two O–H···O bonds. © *The Author(s), 2021. Published by Cambridge University Press on behalf of International Centre for Diffraction Data.*
[doi:10.1017/S0885715621000270]

Key words: dimethylarsinic acid, cacodylic acid, powder diffraction, Rietveld refinement, density functional theory

## I. INTRODUCTION

Dimethylarsinic acid ($DMA^V$), also known by the trivial name cacodylic acid (CAS number 75-60-5), is a common form of organic arsenic with two known crystalline polymorphs having triclinic (Trotter and Zobel, 1965) and monoclinic (Betz *et al.*, 2011) symmetry. Until fairly recently, $DMA^V$ and other organoarsenicals were used as pesticides for crops (Quazi *et al.*, 2013; Nagar *et al.*, 2014), despite abundant evidence of the toxicity of arsenic (Tchounwou *et al.*, 2003; Capitani, 2011). Arsenic (As) is generally considered to be the most impactful environmental toxin (ATSDR, 2020), based on the frequency of occurrence (at American National Priority List sites), toxicity, and potential for human exposure. In addition to the widespread distribution of $DMA^V$ in pesticide polluted soils, arsenic content is a common concern with rice, and $DMA^V$ had been demonstrated to cause straighthead disorder in rice (Limmer *et al.*, 2018). Methods of mitigating $DMA^V$ contamination in the environment are an active area of research (Adamescu *et al.*, 2011; Tofan-Lazar and Al-Abadleh, 2012). $DMA^V$ has been observed in some seafood and fish species (Borak and Hosgood, 2007) and is one of the primary metabolites produced in the body from the ingestion and inhalation of inorganic arsenic compounds (Hughes and Kenyon, 1998).

The monoclinic polymorph of $DMA^V$ was only recently characterized by single-crystal X-ray diffraction (SC-XRD) at 200 K (Betz *et al.*, 2011), and there is no Powder Diffraction File (Gates-Rector and Blanton, 2019) entry for the compound in the standard PDF-4+ database. The structure has been refined in this work with room temperature powder X-ray diffraction (PXRD) data and compared with a density functional theory (DFT)-optimized structure (plus the original single-crystal structure). The original triclinic polymorph structure of $DMA^V$ was also determined by single-crystal X-ray diffraction (Trotter and Zobel, 1965), but without solution of the hydrogen atom positions. An experimental entry for triclinic $DMA^V$ with no structure is present in the database, PDF 00-029-1588 (Gates-Rector and Blanton, 2019). DFT geometry optimization has been used to add hydrogen positions to triclinic $DMA^V$ in this work. The experimental PXRD data for monoclinic $DMA^V$ and the DFT-optimized structure for triclinic $DMA^V$ have been used to generate Bragg reflection lists for inclusion in the PDF.

## II. EXPERIMENTAL

A specimen of $DMA^V$ obtained from Sigma-Aldrich was lightly ground with a mortar and pestle. The specimen was mounted in a 0.3 mm ID polyimide capillary, sealed at both ends with Loctite adhesive.

PXRD patterns were collected using a Canadian Macromolecular Crystallography Facility beamline (08B1-1, Fodje *et al.*, 2014) at the Canadian Light Source (CLS). 08B1-1 is a bending magnet beamline with a Si (111) double-crystal monochromator. Two-dimensional (2D) data were obtained using a Rayonix MX300HE detector with an active area of 300 mm × 300 mm. The patterns were collected at an energy of 18 keV ($\lambda = 0.68919$ Å) and a sample-detector distance of 250 mm.

The 2D PXRD patterns were calibrated and integrated using the GSASII software package (Toby and Von Dreele, 2013). The sample-detector distance, detector centering, tilt, and wavelength were calibrated using a series of patterns obtained from a lanthanum hexaboride ($LaB_6$) standard reference material (NIST SRM 660a $LaB_6$), and the calibration parameters were applied to all patterns. The 2D patterns for $DMA^V$ exhibited minor graininess, bordering on an ideal powder, and based on the minimal grinding, it is believed that the

[a)]Author to whom correspondence should be addressed.
Electronic mail: joel.reid@lightsource.ca

 © 2021 JCPDS-ICDD
https://doi.org/10.1017/S0885715621000270 Published online by Cambridge University Press

TABLE I. The crystal data, data collection, and refinement parameters obtained for monoclinic $DMA^V$.

| | |
|---|---|
| Crystal data | |
| Formula, $Z$ | $(CH_3)_2AsO(OH)$, $Z = 8$ |
| Molar mass | 138.00 g $mol^{-1}$ |
| Symmetry, space group | Monoclinic, $C2/c$ (61) |
| Unit-cell parameters | $a = 15.9264(15)$ Å, $b = 6.53999(8)$ Å, $c = 11.3401(9)$ Å, $\beta = 125.8546(17)°$ |
| Volume | 957.340(12) $Å^3$ |
| Density ($\rho_{calc}$) | 1.915 g $cm^{-3}$ |
| Data collection | |
| Beamline | CLS 08B1-1 |
| Monochromator | Si (111) double-crystal monochromator |
| Detector | Rayonix MX300HE (300 mm × 300 mm) |
| Specimen mounting | 0.3 mm Kapton capillary |
| Collection mode | Transmission |
| Wavelength | $\lambda = 0.68919$ Å |
| Collection range, step size | 2° to 39° (2$\theta$), 0.05°/step (refinement region: 3° to 39°) |
| Refinement | |
| Number of data points | 7200 |
| Background correction | 12-term log interpolate function |
| Number of refined parameters | 39 |
| $R_p$ | 0.00876 |
| $R_{wp}$ | 0.01305 |
| Reduced $\chi^2$ | 1.28 |

monoclinic polymorph of $DMA^V$ was present in the as-received material. After calibration, the 2D patterns were integrated to obtain standard point detector powder diffraction patterns.

Rietveld refinement was performed starting with the single-crystal structure of Betz *et al.* (2011). Rietveld refinements of the crystal structure were performed with the GSASII program (Toby and Von Dreele, 2013) using a Thompson-Cox-Hastings modified pseudo-Voigt peak shape function (Thompson *et al.*, 1987). The background was modeled using a 12-term log interpolation function. Positional parameters were refined with soft restraints on bond distances and angles for the As, C, and O atoms in the $DMA^V$ molecule obtained using Mogul 1.8.3 (Bruno *et al.*, 2004). Hydrogen positions were left fixed during refinement but were periodically optimized using Avogadro (Hanwell *et al.*, 2012). The isotropic displacement parameters of the hydrogen atoms were constrained to be 1.3 times the value of the chemically bonded non-hydrogen atom.

The crystal data, data collection, and refinement details are summarized in Table I.

DFT geometry optimizations were performed on both the monoclinic and triclinic polymorphs of $DMA^V$ using CRYSTAL17 (Dovesi *et al.*, 2018). Basis sets were obtained from the literature for the C, H, O (Gatti *et al.*, 1994), and As atoms (Peintinger *et al.*, 2013). The calculations used the B3LYP functional (Becke, 1993) and D3 dispersion correction (Grimme *et al.*, 2010) with eight *k*-points.

For the DFT-optimized structure of triclinic $DMA^V$, the PXRD pattern was calculated for Bragg–Brentano geometry with Cu$K\alpha_1$ ($\lambda = 1.54059$ Å) radiation using the PowderCell program (Kraus and Nolze, 1996).

## III. RESULTS AND DISCUSSION

The final Rietveld refinement obtained for the synchrotron PXRD data from the monoclinic $DMA^V$ sample is illustrated in Figure 1, whereas the refined atomic coordinates and DFT-optimized atomic coordinates are shown in Tables II and III, respectively. Visually, the refinement looks excellent, and the root-mean-square (RMS) Cartesian displacements between the PXRD, DFT-optimized, and SC-XRD structures are all below 0.1 Å, suggesting excellent agreement between

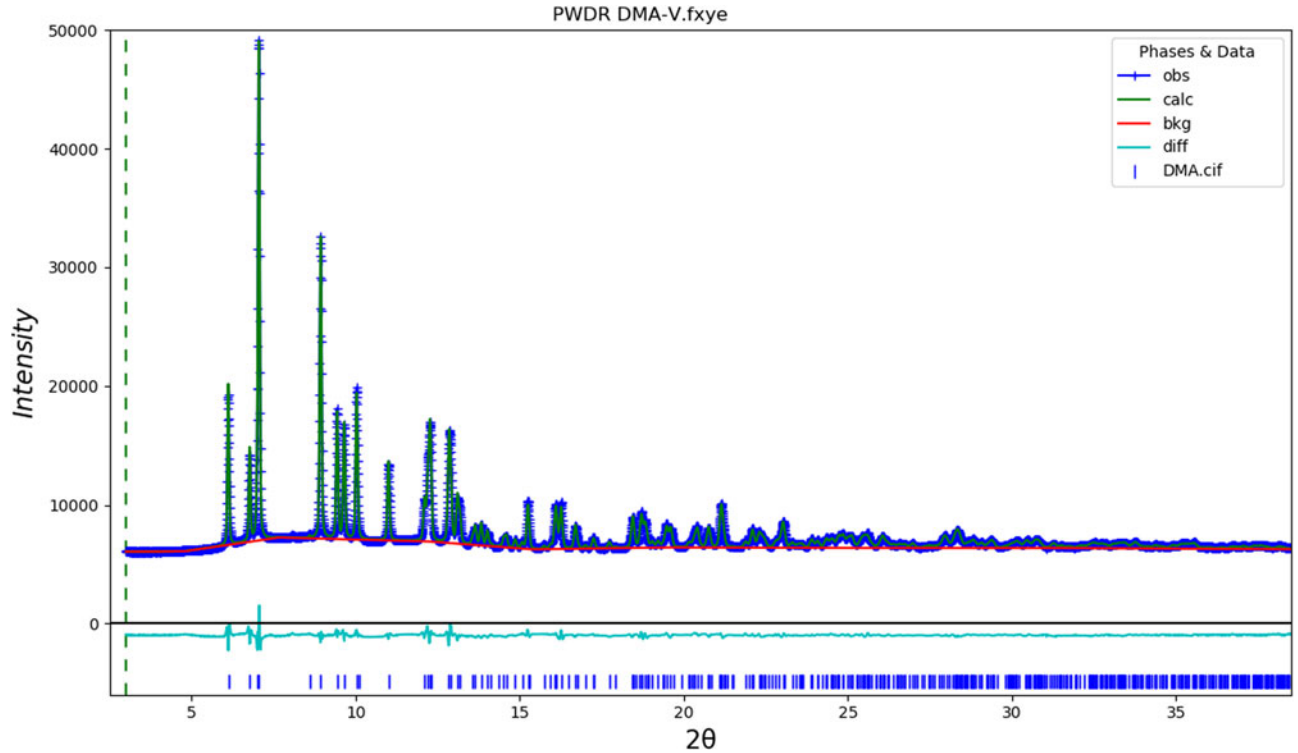



Figure 1. A plot illustrating the final Rietveld refinement for monoclinic $DMA^V$ obtained with GSASII.


https://doi.org/10.1017/S0885715621000270 Published online by Cambridge University Press

TABLE II. The Rietveld-refined crystal structure of monoclinic DMA$^V$ with lattice parameters: $a = 15.9264(15)$ Å, $b = 6.53999(8)$ Å, $c = 11.3401(9)$ Å, and $\beta = 125.8546(17)°$.

| Atom | *x/a* | *y/b* | *z/c* | Wyckoff | $U_{iso}$ (Å$^2$) |
|---|---|---|---|---|---|
| As1 | 0.16236(8) | 0.16043(15) | 0.12681(12) | 8f | 0.0291(4) |
| O2 | 0.12725(26) | 0.0798(5) | 0.5531(4) | 8f | 0.0277(20) |
| O3 | 0.28860(26) | 0.1836(5) | 0.2208(4) | 8f | 0.0190(17) |
| C4 | 0.40633(29) | 0.1620(6) | 0.0382(4) | 8f | 0.0174(17) |
| C5 | 0.11394(28) | 0.2116(6) | 0.2448(4) | 8f | 0.0174 |
| H6 | 0.34451 | 0.2961 | 0.3651 | 8f | 0.036 |
| H7 | 0.1517 | 0.1113 | 0.3396 | 8f | 0.0227 |
| H8 | 0.1308 | 0.3712 | 0.2795 | 8f | 0.0227 |
| H9 | 0.03063 | 0.1831 | 0.1744 | 8f | 0.0227 |
| H10 | 0.3737 | 0.1885 | 0.0991 | 8f | 0.0227 |
| H11 | 0.48937 | 0.1938 | 0.1049 | 8f | 0.0227 |
| H12 | 0.392 | 0.004 | −0.0002 | 8f | 0.0227 |

All atoms were refined with fixed site occupancies of 1.

the structures (Van de Streek and Neumann, 2014). The atom labels used for the structural models are illustrated in Figure 2, and a view of the DFT-optimized structure along the *b*- and *c*-axes are illustrated in Figure 3. The structure is well described by Betz *et al.* (2011) as infinite zigzag chains parallel to the *b*-axis defined by the strong O–H···O hydrogen bonds between the H6 atom of the hydroxyl group (donor) and the double-bonded O3 (acceptor) in the neighboring molecule along the chain. The hydrogen bonds obtained from the DFT optimization have comparable values to the SC-XRD refinement (Betz *et al.*, 2011) and are shown in Table IV.

The DFT-optimized atomic coordinates of triclinic DMA$^V$ are shown in Table V. A molecular overlay of the DFT-optimized structure and the original SC-XRD structure (Trotter and Zobel, 1965) is illustrated in Figure 4. The RMS Cartesian displacement of the non-hydrogen atoms is 0.13 Å, suggesting excellent agreement between the DFT-optimized and original SC-XRD structures (Van de Streek and Neumann, 2014). The DFT-optimized triclinic DMA$^V$ structure is illustrated in Figure 5 along both the *a*- and *b*-axes. Similar to the monoclinic structure, the strongest hydrogen bond is the intermolecular O–H···O bond, but in contrast to the monoclinic DMA$^V$ structure, molecules in triclinic DMA$^V$ form dimers with pairs of O–H···O bonds between them. Weaker intermolecular C–H···O hydrogen bonds provide connections between the dimers. The hydrogen bonds are tabulated in Table IV.

For the experimental PXRD data for monoclinic DMA$^V$, a Bragg reflection list based on the GSASII refinement was prepared by summing reflections closer than 0.02°, 2$\theta$ as multiple reflections and assigning a weighted average reflection position, then including all reflections with relative integrated intensities of 0.2% or greater, up to 30° in 2$\theta$. For the DFT-optimized structure of triclinic DMA$^V$, the Bragg reflection list calculated using PowderCell (Cu$K\alpha_1$, $\lambda = 1.54059$ Å) was edited by summing reflections closer than 0.03° in 2$\theta$ as multiple reflections and assigning them a weighted average reflection position, then including all reflections with relative integrated intensities of 0.2% or greater up to 75° in 2$\theta$. The Bragg reflection lists and raw data are contained in a crystallographic information file (CIF), which have been deposited with ICDD, along with individual CIF files for the Rietveld-refined and DFT-optimized structures.

TABLE III. The DFT-optimized crystal structure of monoclinic DMA$^V$ with fixed lattice parameters: $a = 15.9263$ Å, $b = 6.5402$ Å, $c = 11.3402$ Å, and $\beta = 125.856°$.

| Atom | *x/a* | *y/b* | *z/c* |
|---|---|---|---|
| As1 | 0.16484 | 0.15423 | 0.12656 |
| O2 | 0.12601 | 0.09076 | 0.55194 |
| O3 | 0.29432 | 0.17538 | 0.22735 |
| C4 | 0.40331 | 0.17174 | 0.04143 |
| C5 | 0.11235 | 0.20485 | 0.23904 |
| H6 | 0.34327 | 0.30699 | 0.36388 |
| H7 | 0.15011 | 0.10458 | 0.33381 |
| H8 | 0.12921 | 0.36449 | 0.27370 |
| H9 | 0.02904 | 0.17637 | 0.16867 |
| H10 | 0.37068 | 0.19821 | 0.10234 |
| H11 | 0.48635 | 0.20350 | 0.10816 |
| H12 | 0.38898 | 0.01371 | 0.00311 |

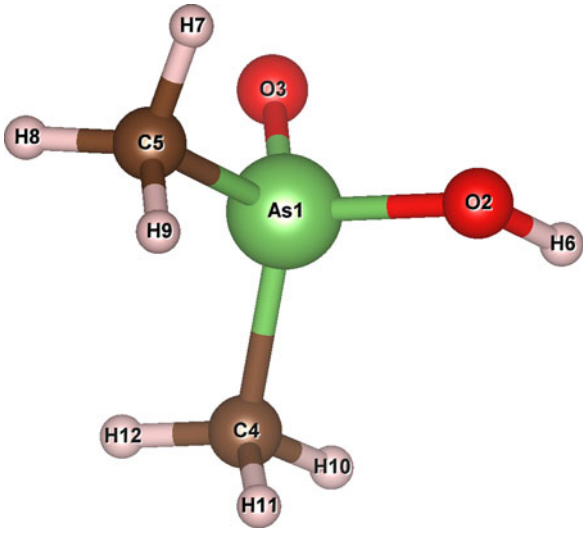



Figure 2. The atom labels used for structure description of DMA$^V$. The figure was prepared with VESTA (Momma and Izumi, 2011).


https://doi.org/10.1017/S0885715621000270 Published online by Cambridge University Press

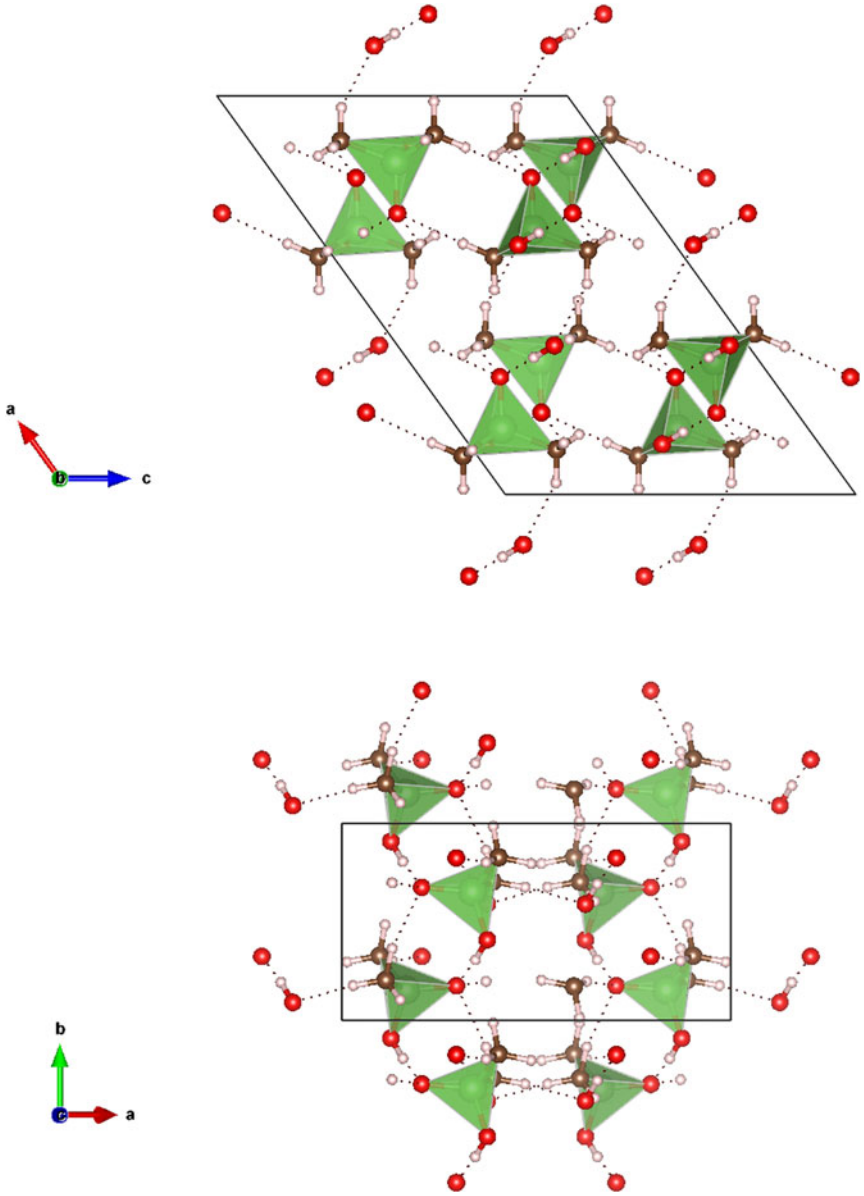



Figure 3. The DFT-optimized crystal structure of monoclinic $DMA^V$, viewed along the *b*-axis (top) and *c*-axis (bottom). The atom types can be identified by color including arsenic (green tetrahedra), carbon (brown), oxygen (red), and hydrogen (pink). Hydrogen bonds are represented by the dotted lines. The unit cell is outlined in black. The figure was prepared with VESTA (Momma and Izumi, 2011).

## IV. DEPOSITED DATA

The Crystallographic Information Framework (CIF) files containing the results of the Rietveld refinement (including the raw data) and the DFT geometry optimizations were deposited with ICDD. The data can be requested at info@icdd.com.

TABLE IV. The most prominent hydrogen bonds observed in the two $DMA^V$ structures and their parameters obtained from the DFT modeling.

| H-Bond | D-H (Å) | H···A (Å) | D···A (Å) | D-H···A (°) |
|---|---|---|---|---|
| Monoclinic $DMA^V$ | | | | |
| O2–H6···O3 | 1.025 | 1.527 | 2.548 | 173.6 |
| C4–H10···O3 | 1.094 | 2.352 | 3.427 | 167.1 |
| C5–H9···O2 | 1.092 | 2.331 | 3.344 | 153.6 |
| Triclinic $DMA^V$ | | | | |
| O2–H6···O3 | 1.030 | 1.522 | 2.550 | 175.4 |
| C4–H12···O3 | 1.091 | 2.423 | 3.348 | 141.6 |
| C5–H7···O2 | 1.093 | 2.420 | 3.510 | 174.7 |

TABLE V. The DFT-optimized crystal structure of triclinic $DMA^V$ with fixed lattice parameters: $a = 6.1852$Å, $b = 6.5300$ Å, $c = 6.6100$ Å, $\alpha = 101.240°$, $\beta = 91.884°$, and $\gamma = 115.193°$.

| Atom | *x*/*a* | *y*/*b* | *z*/*c* |
|---|---|---|---|
| As1 | 0.06552 | 0.20808 | 0.30487 |
| O2 | 0.12251 | −0.02380 | 0.24191 |
| O3 | 0.14168 | 0.33210 | −0.42665 |
| C4 | 0.26582 | 0.46014 | 0.18749 |
| C5 | −0.26992 | 0.12386 | 0.23800 |
| H6 | 0.03618 | 0.21396 | −0.34593 |
| H7 | −0.37539 | −0.00959 | 0.31865 |
| H8 | −0.31246 | 0.05704 | 0.06968 |
| H9 | −0.29910 | 0.27840 | 0.28735 |
| H10 | 0.45298 | −0.47994 | 0.25255 |
| H11 | 0.21194 | −0.39953 | 0.22744 |
| H12 | 0.23900 | 0.39560 | 0.01913 |


https://doi.org/10.1017/S0885715621000270 Published online by Cambridge University Press

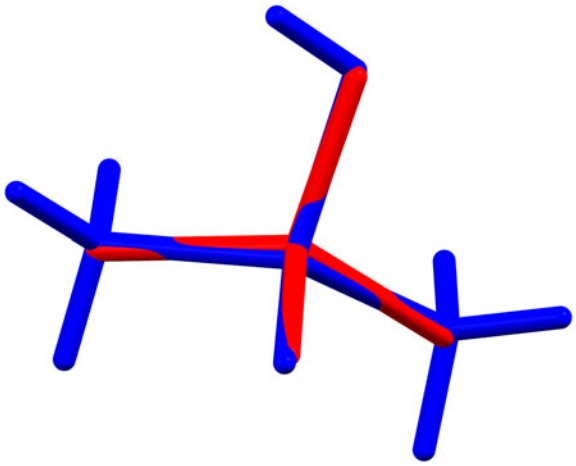


Figure 4. A molecular overlay of the original SC-XRD structure (Trotter and Zobel, 1965) of triclinic $DMA^V$, with no hydrogen atoms, in red, and the DFT-optimized structure, with hydrogen atoms, in blue. The RMS Cartesian displacement of the non-hydrogen atoms is 0.13 Å. The figure was prepared with Mercury (Macrae *et al.*, 2008).

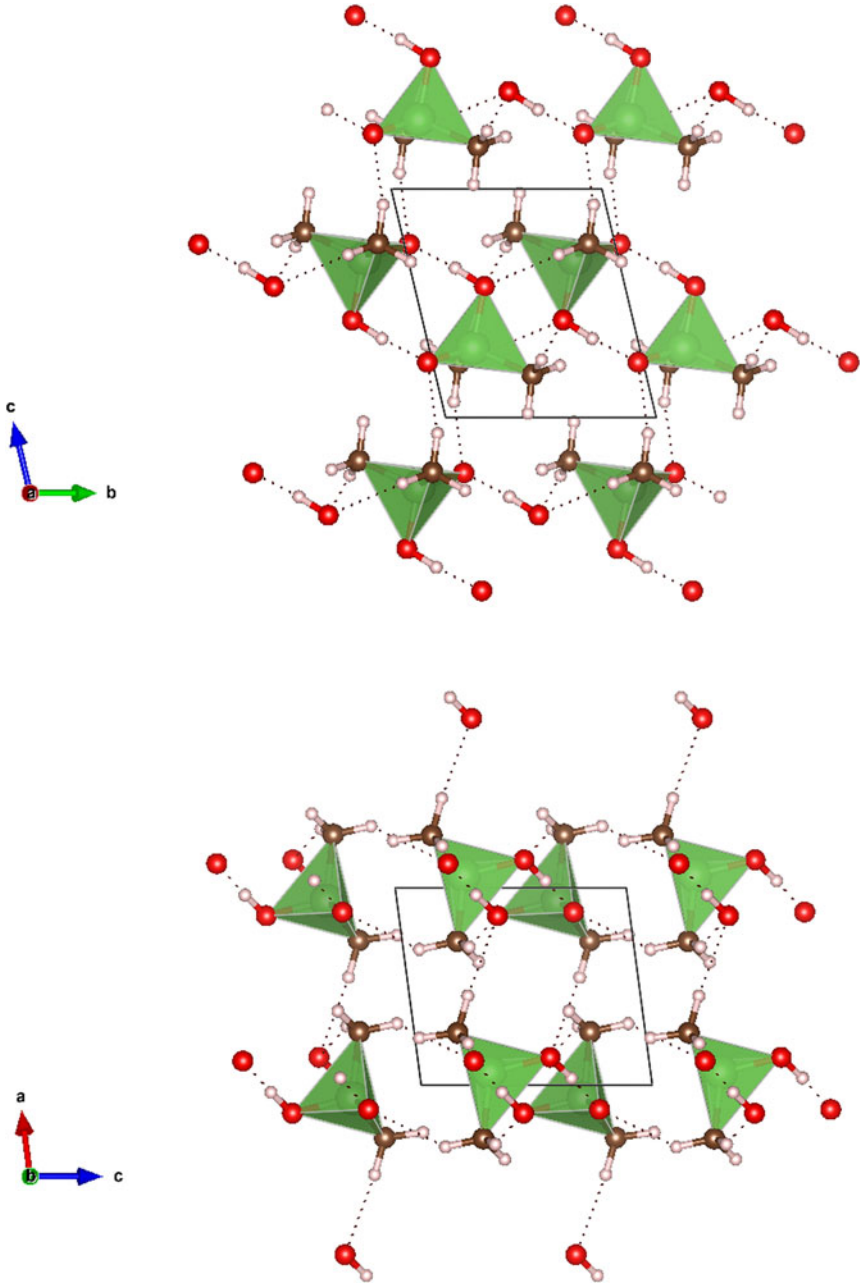



Figure 5. The DFT crystal structure of triclinic $DMA^V$, viewed along the *a*-axis (top) and *b*-axis (bottom). The atom types can be identified by color including arsenic (green tetrahedra), carbon (brown), oxygen (red), and hydrogen (pink). Hydrogen bonds are represented by the dotted lines. The unit cell is outlined in black. The figure was prepared with VESTA (Momma and Izumi, 2011).


## ACKNOWLEDGEMENTS

Many thanks are due to Jim Kaduk for helpful discussions regarding density functional theory and the CRYSTAL software package, and for providing a constant source of inspiration.

Research described in this paper was performed using beamline 08B1-1 at the Canadian Light Source, which is supported by the Canadian Foundation for Innovation, the Natural Sciences and Engineering Research Council of Canada, the National Research Council Canada, the Canadian Institutes of Health Research, the Government of Saskatchewan, Western Economic Diversification Canada, and the University of Saskatchewan.




https://doi.org/10.1017/S0885715621000270 Published online by Cambridge University Press

Adamescu, A., Hamilton, I. P., and Al-Abadleh, H. A. (**2011**). "Thermodynamics of dimethylarsinic acid and arsenate interactions with hydrated iron-(oxyhydr)oxide clusters: DFT calculations," Environ. Sci. Technol. **45**, 10438–10444.

Agency for Toxic Substances and Disease Registry, ATSDR (**2020**). Priority list of hazardous substances. Available at: http://www.atsdr.cdc.gov/SPL/index.html.

Becke, A. D. (**1993**). "Density-functional thermochemistry. III. The role of exact exchange," J. Chem. Phys. **98**, 5648–5652.

Betz, R., McCleland, C., and Marchand, H. (**2011**). "The monoclinic polymorph of dimethyl-arsinic acid," Acta Crystallogr. E **E67**, m1013.

Borak, J. and Hosgood, H. D. (**2007**). "Seafood arsenic: implications for human risk assessment," Regul. Toxicol. Pharmacol. **47**, 204–212.

Bruno, I. J., Cole, J. C., Kessler, M., Luo, J., Motherwell, W. D. S., Purkis, L. H., Smith, B. R., Taylor, R., Cooper, R. I., Harris, S. E., and Orpen, A. G. (**2004**). "Retrieval of crystallographically-derived molecular geometry information," J. Chem. Inf. Comput. Sci. **44**, 2133–2144.

Capitani, E. M. D. (**2011**). "Arsenic toxicology - a review," in *Arsenic: Natural and Anthropogenic*, edited by F. Deschamps and J. Matschullat (CRC Press, London), pp. 27–37.

Dovesi, R., Erba, A., Orlando, R., Zicovich-Wilson, C. M., Civalleri, B., Maschio, L., Rerat, M., Casassa, S., Baima, J., Salustro, S., and Kirtman, B. (**2018**). "Quantum-mechanical condensed matter simulations with CRYSTAL," WIREs Comput. Mol. Sci. **8**, e1360.

Fodje, M., Grochulski, P., Janzen, K., Labiuk, S., Gorin, J., and Berg, R. (**2014**). "08B1-1: an automated beamline for macromolecular crystallography experiments at the Canadian Light Source," J. Synchrotron Radiat. **21**, 633–637.

Gates-Rector, S. D. and Blanton, T. N. (**2019**). "The Powder Diffraction File: a quality materials characterization database," Powd. Diffr. **34**, 352–360.

Gatti, C., Saunders, V. R., and Roetti, C. (**1994**). "Crystal-field effects on the topological properties of the electron-density inmolecular crystals - the case of urea," J. Chem. Phys **101**, 10686–10696.

Grimme, S., Antony, J., Ehrlich, S., and Krieg, H. (**2010**). "A consistent and accurate *ab initio* parameterization of density functional dispersion correction (DFT-D) for the 94 elements H-Pu," J. Chem. Phys. **132**, 154104.

Hanwell, M. D., Curtis, D. E., Lonie, D. C., Vandermeersch, T., Zurek, E., and Hutchison, G. R. (**2012**). "Avogadro: an advanced semantic chemical editor, visualization, and analysis platform," J. Cheminform. **4**, 17.

Hughes, M. F. and Kenyon, E. M. (**1998**). "Dose-dependent effects on the disposition of monomethylarsonic acid and dimethylarsinic acid in the mouse after intravenous administration," J. Toxicol. Environ. Health A **53**, 95–112.

Kraus, W. and Nolze, G. (**1996**). "POWDER CELL – a program for the representation and manipulation of crystal structures and calculation of the resulting X-ray powder patterns," J. Appl. Crystallogr. **29**, 301–303.

Limmer, M. A., Wise, P., Dykes, G. E., and Seyfferth, A. L. (**2018**). "Silicon decreases dimethylarsinic acid concentration in rice grain and mitigates straighthead disorder," Environ. Sci. Technol. **52**, 4809–4816.

Macrae, C. F., Bruno, I. J., Chisholm, J. A., Edgington, P. R., McCabe, P., Pidcock, E., Rodriquez-Monge, L., Taylor, R., van de Streek, J., and Wood, P. A. (**2008**). "Mercury CSD 2.0 – new features for the visualization and investigation of crystal structures," J. Appl. Crystallogr. **41**, 466–470.

Momma, K. and Izumi, F. (**2011**). "VESTA 3 for three-dimensional visualization of crystal, volumetric and morphology data," J. Appl. Crystallogr. **44**, 1272–1276.

Nagar, R., Sarkar, D., Makris, K., and Datta, R. (**2014**). "Arsenic bioaccessibility and speciation in the soils amended with organoarsenicals and drinking-water treatment residuals based on a long-term greenhouse study," J. Hydrol. **518**, 477–485.

Peintinger, M. F., Vilela Oliveira, D., and Bredow, T. (**2013**). "Consistent Gaussian basis sets of triple-zeta valence with polarization quality for solid-state calculations," J. Comput. Chem. **34**, 451–459.

Quazi, S., Sarkar, D., and Datta, R. (**2013**). "Human health risk from arsenical pesticide contaminated soils: a long-term greenhouse study," J. Hazard. Mater. **262**, 1031–1038.

Tchounwou, P. B., Patlolla, A. K., and Centeno, J. A. (**2003**). "Carcinogenic and systemic health effects associated with arsenic exposure—a critical review," Toxicol. Pathol. **31**, 575–588.

Thompson, P., Cox, D. E., and Hastings, J. B. (**1987**). "Rietveld refinement of Debye-Scherrer synchrotron X-ray data from $A1_2O_3$," J. Appl. Crystallogr. **20**, 79–83.

Toby, B. H. and Von Dreele, R. B. (**2013**). "GSAS II: the genesis of a modern open-source all-purpose crystallography software package," J. Appl. Crystallogr. **46**, 544–549.

Tofan-Lazar, J. and Al-Abadleh, H. A. (**2012**). "ATR-FTIR studies on the adsorption/desorption kinetics of dimethylarsinic acid on iron−(oxyhydr)oxides," J. Phys. Chem. A **116**, 1596–1604.

Trotter, J. and Zobel, T. (**1965**). "Stereochemistry of arsenic. Part XVI. Cacodylic acid," J. Chem. Soc., 4466–4471.

Van de Streek, J. and Neumann, M. A. (**2014**). "Validation of molecular crystal structures from powder diffraction data with dispersion corrected density functional theory (DFT-D)," Acta Crystallogr. B. **70**, 1020–1032.



https://doi.org/10.1017/S0885715621000270 Published online by Cambridge University Press